Journal of Materials and Environmental Science
ISSN : 2028-2508
e-ISSN : 2737-890X
CODEN : JMESCN

J. Mater. Environ. Sci., 2023, Volume 14, Issue 11, Page 1148-1159

http://www.jmaterenvironsci.com

Effect of precursor temperature on electrochemically deposited zirconium doped chromium telluride using a standard three-electrode system

Ernest O. Ojegu[1], Ogo B. Odia[1], Mike O. Osiele[1], Akpojotor E. Godfrey[1], Imosobomeh L. Ikhioya[2, 3]

[1]Department of Physics, Delta State University, Abraka. Delta State, Nigeria
[2]Department of Physics and Astronomy, University of Nigeria, Nsukka, 410001, Enugu State, Nigeria
[3]National Centre for Physics, Quaid-i-Azam University Campus, Islamabad, 44000, Pakistan
Corresponding author, Email address: imosobomeh.ikhioya@unn.edu.ng, https://orcid.org/0000-0002-5959-4427

Received *22 Sept 2023,* ***Revised*** *28 Oct 2023,* ***Accepted*** *30 xxx 2023*

Keywords:
- ✓ *chromium;*
- ✓ *zirconium;*
- ✓ *doping;*
- ✓ *bandgap;*
- ✓ *precursor temperature;*

Citation*: Ojegu E. O., Odia O. B., Mike O. Osiele M. O., Godfrey A. E., Ikhioya I. L. (2023) Effect of precursor temperature on electrochemically deposited zirconium doped chromium telluride using a standard three-electrode system, J. Mater. Environ. Sci., 14(11), 1148-1159*

Abstract: We have used electrochemical deposition to synthesize CrTe and Zr/CrTe by modifying the precursor temperature of the films. The material showed a prominent peak at orientation (121), which corresponds to a 2theta value of 46.92o, together with a flawless hexagonal phase diffraction plane that is classified to orientations (111), (112), (121), and (200), corresponding to 2theta values of 21.57o, 32.20o, 46.92o, and 60.02o. The films exhibit a drop in resistivity and a rise in thickness from 104.02 to 109.23 nm. The undoped film's reflectance is highest in the visible region and gradually decreases until it approaches the near-infrared region. The reflectance of the films decreases in the UV region while the precursor temperatures rise along with the increase in reflectance in the visible area. The CrTe image shows a well-packed shaving surface with condensed particles. The surface morphology of the films has revealed the smote surface with obvious stone dot micro grain that was detected as the precursor reaches a temperature of 50°C. The CrTe pristine has a bandgap energy of 1.62 eV, and Zr/CrTe synthesized at a different precursor temperature, has a bandgap energy of 1.73-1.68 eV, demonstrating that as the precursor temperature rises, the energy bandgap decreases.

1. Introduction

Energy is a major resource for human activities and plays a significant role in our daily lives. To save energy, technologies like light-emitting diodes, fuel cells, lithium-ion batteries, solar cells, and ultra-capacitors were utilized. Future energy storage systems, transmission, and generation are predicted to benefit from the use of nanotechnology since they will be more affordable and effective (Hala., 2023; Arbouch *et al.* 2014). In various applications, including solar thermal systems, solar photovoltaic systems, hydrogen production, novel devices with high efficiency, energy-saving technologies, low energy consumption, and low cost may be produced by the manufacturing of materials and structures at the nanoscale (Jafari *et al.* 2023). New uses for nanotechnology are emerging quickly in numerous industries. By creating nanosystems, nanostructures, and nanomaterials, for instance, nano-engineering opens up new possibilities for advancement in a variety of industries, including agriculture, food

processing, healthcare, construction, environmental protection, and energy (Barhoum *et al.*, 2022). The creation of numerous different nanoparticles and nanostructured materials, as well as their use in related applications ranging from the development of new nanomaterials to the direct control of matter at the atomic level, are currently impacted by a variety of research fields, from semiconductor physics to organic chemistry. Because of their distinctive features, nanostructured materials have drawn a lot of attention in the fabrication of nano-devices for various purposes (Mobeen *et al.*, 2022). Because of the quantum confinement phenomena that take place during size reduction, nanomaterials have distinctive mechanical, and optical properties, and electrical, and chemical. The development of novel gadgets with a wide range of applications that use low energy consumption, cheap cost, and high efficiency has the potential to utilize nanoscale materials and structures. Energy-related technologies such as fuel cells, lighting, lithium-ion batteries, solar thermal systems, and solar photovoltaic systems all contribute to the conversion and storage of renewable energy (Mote *et al.*, 2015). One dimension at the nanoscale, like a surface coating adhered to a substrate, is demonstrated by the nanomaterials created from various materials. In contrast, two-dimensional nanomaterials are often applied with nanoparticles, Nanoporous thin films and wires or tubes made of alumina on a surface, small nanostructures can be used to show three-dimensional nanomaterials (Polat *et al.*, 2019).

Doping is an effective and convenient way to change the parent materials' optical characteristics. Additionally, doping will increase the spectrum of applications for basic materials. Doping is the addition of a dopant to a semiconductor that causes the Fermi levels to shift (Mote *et al.*, 2015, Polat *et al.*, 2019). Due to its low cost, non-toxic, high transparency, and exceptional optoelectronic capabilities, the zirconium-doped chromium telluride material attracted a lot of attention. Sven *et al.*, (2002) deposited thin layers of chromium and tellurium superlattice reactants on a Si-(100) film and observed the reactions with in-situ and ex-situ XRD as well as X-ray reflectometry. The films' compositions ranged from 71 to 86 percent Te, and the number of layers was altered between 3 and 653. At a temperature of roughly 300°C, films with thick Cr/Te two-layers (300-3000) react to produce high-textured and crystalline (h00)-CrTe3. Using several Cr-Te layers that exhibit Cr/Te two layers with a thickness of less than 25, the temperature of formation is significantly lowered to 100ºC. At around 275°C, (h00)-$CrTe_3$ decomposes, and then Cr_2Te_3 crystallizes, forming a functionalized material having a (00l)-texture. Both compounds are stable across a range of temperatures. The mono-chromium tri-telluride decomposed into Cr_2Te_3 only utilizing the thin film samples; no such breakdown could be demonstrated for the thick superlattices. They also show the exceptionally extensive analysis of a sample consisting of six Cr/Te two-layers (Sven *et al.*, 2002). Hui and Leong, (2013) used molecular beam epitaxy to create a rock-salt CrTe thin layer on a MgO substrate. A 50 nm thick metastable rock-salt CrTe thin is forming in a crystalline phase, to investigations using high-resolution transmission electron microscopy. Ferromagnetic transitions take place at two temperatures: 165 K and > 400 K, according to its temperature dependence of residual magnetization. The two-transition temperatures are most likely the result of multi-axial anisotropy in rock salt CrTe. The residual stress at 400 K is examined. it is discovered that the CrTe film contains a novel magnetic phase An electrodeposition approach for the production of CrTe thin films looks to offer significant promise taking into consideration the benefits of a thin film over a bulk powder form for the majority of applications. In this sense, it's crucial to remember that electrochemical deposition offers numerous benefits, including not requiring hazardous chemicals, being economical, using mild synthesis conditions, and being straightforward (Ikhioya *et al.*, 2020, Ikhioya *et al.*, 2019, Ikhioya *et al.*, 2020b, Ikhioya *et al.*, 2014, Wang *et al.*, 2011, Ikhioya *et al.*, 2015, Ikhioya *et al.*, 2018, Ikhioya *et al.*, 2023 Udofia *et al.*, 2022). To create chromium telluride and chromium telluride doped with zirconium,

electrochemical deposition was used. To the best of our knowledge, no attempts have been undertaken to synthesize CrTe and Zr/CrTe material using the electrochemical deposition approach (Yang *et al.*, 2023, Zhang *et al.*, 2022, Jiang *et al.*, 2021, Chen *et al.*, 2022, Sun *et al.*, 2022, Wang *et al.*, 2023, Yang *et al.*, 2023, Luo *et al.*, 2022, Yuxi *et al.*, 2021, Sreenivasan *et al.*, 2006, Hongxi *et al.*, 2019). This paper presents the electrochemical deposition of chromium telluride and zirconium-doped chromium telluride. The temperature of the precursor was optimized. By analyzing the morphology and crystal structure of the CrTe and Zr/CrTe films using X-ray diffraction, X-ray diffraction, energy dispersive X-ray, and scanning electron microscopy we also provide a thorough evaluation of the deposition process.

2. Experimental procedure for the synthesis of chromium telluride and zirconium-doped chromium telluride deposition

Films of chromium telluride and zirconium-doped chromium telluride were deposited on the FTO substrate, which has a sheet resistance of roughly 15.5 Ω/m. The FTO-immersed region covered an area of around 2.5 cm^2. FTO glasses were cleaned in a succession of ultrasonic baths using ethanol, acetone, distilled water, and ammonia water for 15 minutes before the deposition operation. After that, the glasses were placed in an electric thermostatic oven at 65 °C to dry. The electrochemical deposition of chromium telluride and zirconium doped chromium telluride was performed using a 20/25 ml electrolyte solution containing (0.1 M, 10 mL) of chromium (III) chloride ($CrCl_3.6H_2O$) (Sigma Aldrich, 99.9%), (0.1 M, 10 mL) of tellurium dioxide (TeO_2) (Sigma Aldrich, 99%), and (0.2 M, 5 mL) of zirconium (IV) oxychloride octahydrate ($ZrOCl_2.8H_2O$) (Sigma Aldrich, 99.9%) was used to conduct the electrochemical deposition of chromium telluride and zirconium doped chromium telluride. The electrochemical deposition setup involved a direct current (DC) supply to a typical three-electrode cell made up of an Ag/AgCl reference electrode (RE), a platinum counter electrode (CE), and a working electrode made of fluorine-doped tin oxide (FTO) glasses (WE) (Figure 1). The constant voltage was 10 V, and the deposition period was 5 s. The synthesized chromium telluride and zirconium doped chromium telluride films were examined at precursor temperature of (45 – 55) ^oC and 5.8 pH using a -210 mV against a saturated calomel electrode for 5 s under a potentiostat window. While the deposition process was occurring at a potential of 10 V, the solvents in a 50 ml beaker.

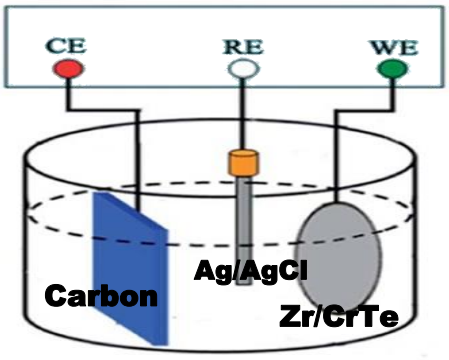

Figure 1: Schematic illustration of the electrochemical deposition technique

The electrochemical bath set-up required modifying the precursor temperature (45 – 50) ^oC in stages. The bath system was filled with 10 mL of the ($CrCl_3.6H_2O$, TeO_2) and 5 mL of $ZrOCl_2.8H_2O$ precursor. The resulting films were then heated to 320 ^oC for 35 min to release the material's tension. The structural properties of the deposited chromium telluride and zirconium doped chromium telluride films were identified using a multi-purpose X-ray diffractometer D8-Advance from Bruker that was

operated in a continuous-scan in locked coupled mode with Cu-Kα radiation (ʎ = 1.5406 Å)., to analyses the surface morphology of the films, scanning electron microscopy was performed. The 756S UV- Visible spectrophotometer was used to calculate the absorbance wavelength at the optical spectral for the ranges of 300 nm to 1100 nm. The optical spectral analysis of the absorbance values was used to infer the additional optical and solid-state features, and the Jandel four-point probes method was used to analyses the electrical properties of the films.

3. Results and discussions

3.1 XRD study of CrTe and Zr/CrTe

Figure 2 displays the XRD pattern of CrTe and Zr/CrTe at various precursor temperatures. The materials used to synthesize the films are polycrystalline. The material showed a prominent peak at orientation (121), which corresponds to a 2theta value of 46.92º, together with a flawless hexagonal phase diffraction plane that is classified to orientations (111), (112), (121), and (200), which correspond to 2theta values of 21.57º, 32.20º, 46.92º, and 60.02º. An intensity peak indicates the crystal structure reduction that occurs at larger 2theta degree values; the substrate used for the deposition caused an unindexed peak. Polycrystalline materials are always more effective in producing photovoltaic and solar systems because of their nature. The pattern indicates that the thicker coating and higher precursor temperature may be the causes of the higher peaks, which enhance its surface area for solar and photovoltaic activities. Table 1 contains the average crystallite size, calculated grain sizes and the material's spectrum characteristics.

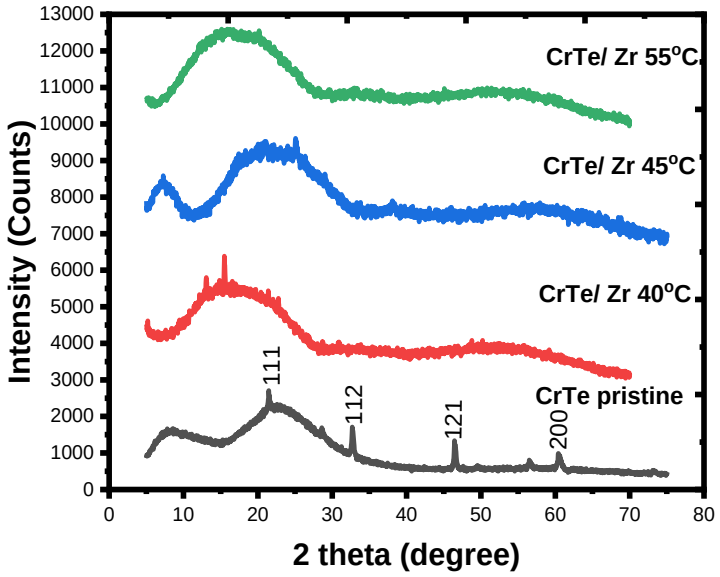

Figure 2: CrTe and Zr/CrTe XRD pattern

Table 1: Structural parameters of CrTe and Zr/CrTe films

Films	2θ (deg.)	(hkl)	Å	a (Å)	(β)	D (nm)
CrTe pristine	21.5721	111	4.1155	7.1284	0.1851	7.6226
CrTe/Zr 45°C	32.2085	112	2.7766	5.5532	0.2095	6.8860
CrTe/Zr 50°C	46.9278	121	1.9343	3.8687	0.1481	6.2132
CrTe/Zr 55°C	60.0292	200	1.5397	3.4429	0.2258	6.0905

3.2 Resistivity and conductivity study of CrTe and Zr/CrTe

The resistivity and conductivity of chromium telluride and chromium telluride-doped zirconium synthesized at different precursor temperatures are shown in Table 2. The films show a rise in thickness from 104.02 to 109.23 nm and a decrease in film resistivity from 7.68 x 10^{-3} to 7.34 x 10^{-3} ohm.m, which further led to an increase in conductivity from 1.30 x 10^{6} to 1.36 x 10^{-3} S/m. The high resistivity and low conductivity of the synthesized films made them suitable for photovoltaic and solar cell applications. Figure 3 (N1) demonstrates high resistivity and low conductivity as the film thickness increases. Resistivity and conductivity are plotted against precursor temperature in Figure 3 (N2), which provides a nonlinear graph and demonstrates how resistivity and conductivity increase and decrease as the precursor temperature increases.

Table 2: Electrical properties of chromium telluride and chromium telluride doped zirconium

Films	t (nm)	**ρ** (Ω.m)	**σ** (S/m)
CrTe	104.02	5.49 x 10^{-3}	1.82 x 10^{6}
CrTe/Zr 45^{0}C	108.15	7.68 x 10^{-3}	1.30 x 10^{6}
CrTe/Zr 50^{0}C	109.00	7.47 x 10^{-3}	1.33 x 10^{6}
CrTe/Zr 55^{0}C	109.23	7.34 x 10^{-3}	1.36x 10^{6}

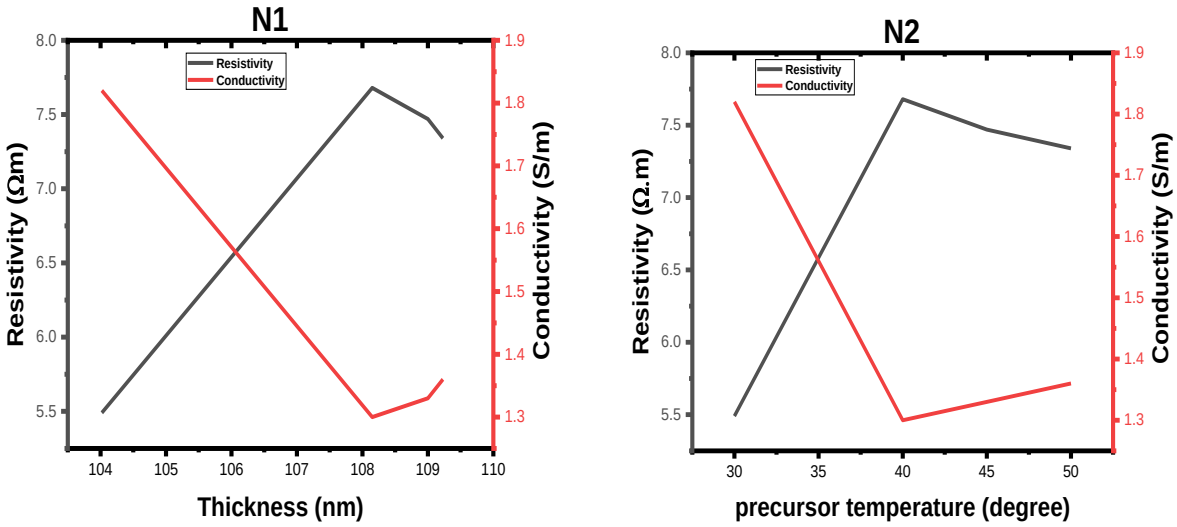

Figure 3: (N1-resistivity &conductivity against films thickness) and (N2-resistivity &conductivity against precursor temperature)

3.3 Optical analysis of chromium telluride and chromium telluride doped zirconium

In Figure 4 (N3), the absorbance spectra of CrTe and Zr/CrTe produced at various precursor temperatures are displayed. The material's'absorption decreases as the light radiation's'wavelength rises. The absorption of the undoped film is maximum in the UV area and gradually falls toward the NIN region. The doped films rise as the precursor temperature of the films increase in both regions. The absorbance of doped material is suited for the industrial manufacture of solar panels for photovoltaic applications since it has a modest absorbance in both spectral areas. Figure 4 (N4) shows the transmittance spectra of CrTe and Zr/CrTe produced at various precursor temperatures. The transmittance of the films increases as its wavelength of the incident light radiation rises.

The transmittance of the undoped film is lowest in the visible area and rises until it reaches the near-infrared region. As the precursor temperatures of the films rise in the UV region, the doped films rise as well, whereas the precursor temperatures of the films fall in the visible area. The doped material's transmittance is moderate in both spectral regions, making it suitable for use in the production of solar panels for photovoltaic applications Figure 4 (N5) shows the reflectance spectra of CrTe and Zr/CrTe synthesized at various precursor temperatures. The reflectance of the films increases together with the wavelength of the incident UV light energy. The undoped film's reflectance is highest in the visible region and gradually decreases until it approaches the near-infrared region. The reflectance of the films decreases in the UV region while the precursor temperatures rise along with the increase in reflectance in the visible area. Doped materials have modest reflectance in both spectral areas, making them appropriate for use in the production of solar panels for photovoltaic applications. Figure 4 (N5) spectra depict the produced films at various precursor temperature energy bandgaps. In contrast to Zr/CrTe synthesized at a different precursor temperature, which has a bandgap energy of 1.73–1.68 eV, the CrTe pristine has a bandgap energy of 1.62 eV, showing that as the precursor temperature rises, the energy bandgap drops. Spectra that displayed the extrapolation of the absorption coefficient square against photon energy demonstrated this.

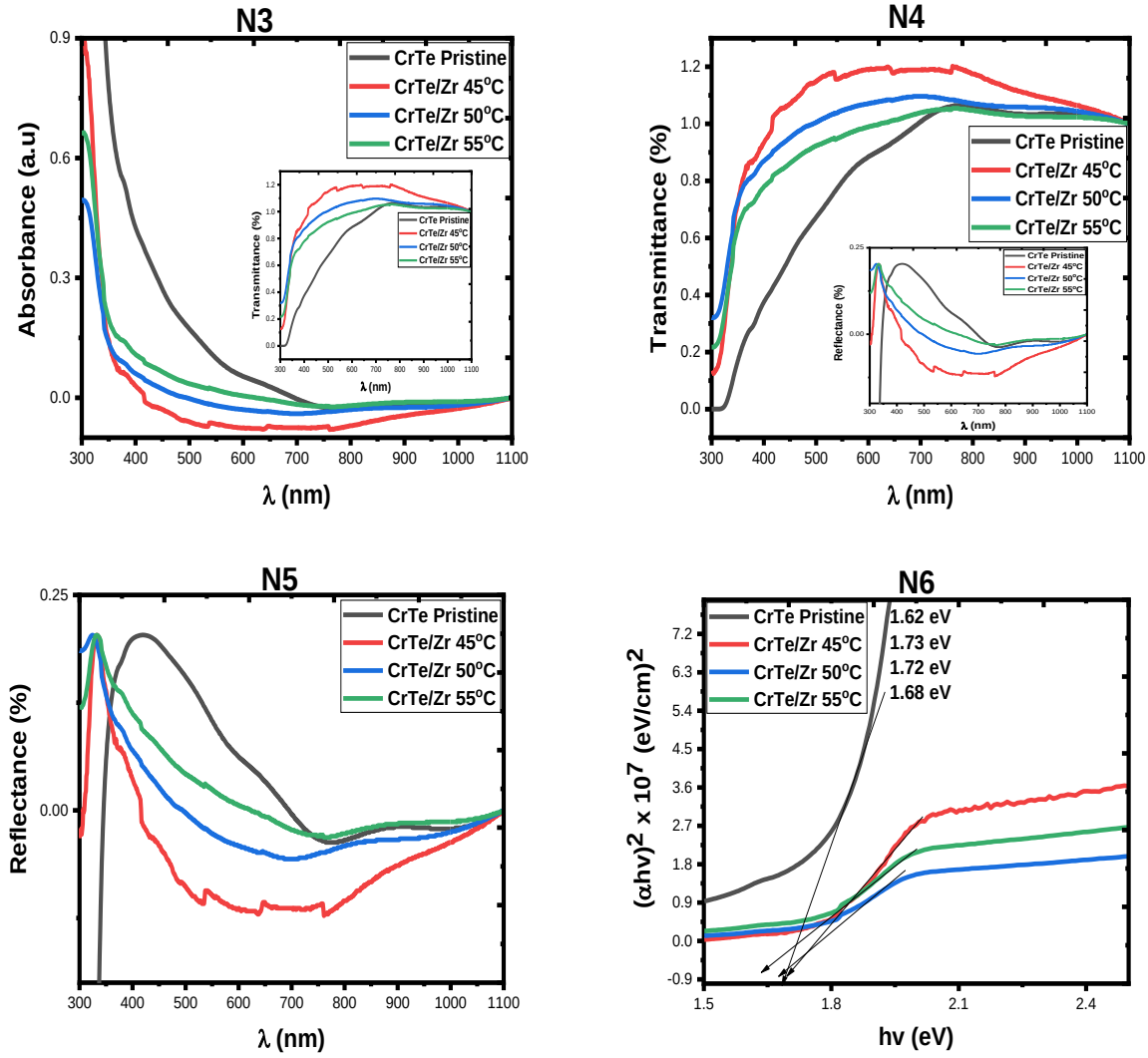

Figure 4: (N3-absorbance), (N4-transmittance), (N5-reflectance), and N6-energy bandgap)

Figure 5 (N7) displays the films' refraction index. Due to the rise in precursor temperature, the films' refractive index shows a rapid increase. The undoped film was found to have the highest refractive index in the visible portion of the spectra. As the photon energy rises, the refractive index of the doped films rises. These show the significant influence that precursor temperature has on synthesized films, as shown in the spectra. The increased refractive index of the films is appropriate for photovoltaic applications because solar panels and lighting systems for electronic sectors require lower refractive indexes. The refractive index of the films increases with increasing precursor temperature. Figure 5 (N8) and (N9) display the films' extinct. Coeff. and optical conductivity. Due to the rise in precursor temperature, the optical conduct. and extinct. Coeff. of the films shows a rapid increase. The highest extinct. coeff. and optical conduct. were found in the visible region of the spectra for the undoped material. As the photon energy rises, the doped films' extinct. coeff. and optical conduct. rise. These show the spectra as well as the considerable effect of precursor temperature on produced films. Because solar panels and lighting systems for the electronic industry need lower extinct. coeff. and optical conduct., the films' extinct. coeff. and optical conduct. rises with rising precursor temperature. Figure 6 (N10) displays the real dielect. const. of the films.

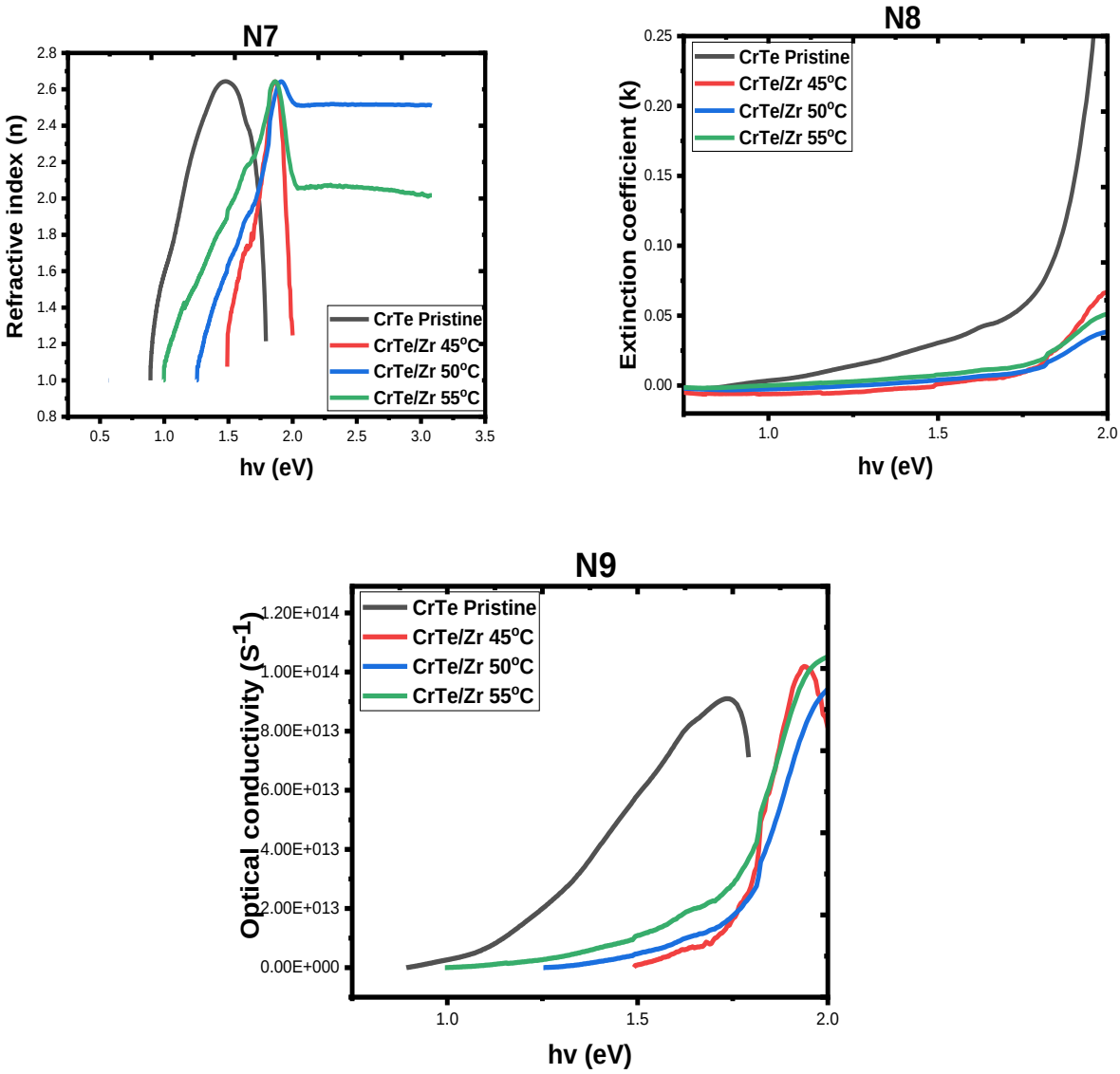

Figure 5: (N7-refractive index), (N8- extinction coefficient), and (N9-optical conductivity)

As the precursor temperature rises, the real dielect. const. of the films shows a significant increase. It was discovered from the spectra that the undoped film has the highest real dielect. const. in the visible portion of the spectrum. As the photon energy rises, the real dielect. const. of the doped films rises. These show the significant influence that precursor temperature has on synthesized films, as shown in the spectra. The increased real dielect. const. of the films is appropriate for photovoltaic applications since solar panels and electronic lighting systems need a lower real dielect. const.. The real dielect. const. of the films increases with increasing precursor temperature. Due to the higher photon energy of the films in Figure 6 (N11), the imag. dielect. const. of the films exhibits a dramatic increase (Al-Ghamdi *et al.*, 2010; Su *et al.* 2021). It was discovered that as the precursor temperature increased, the films' imag. dielect. const.

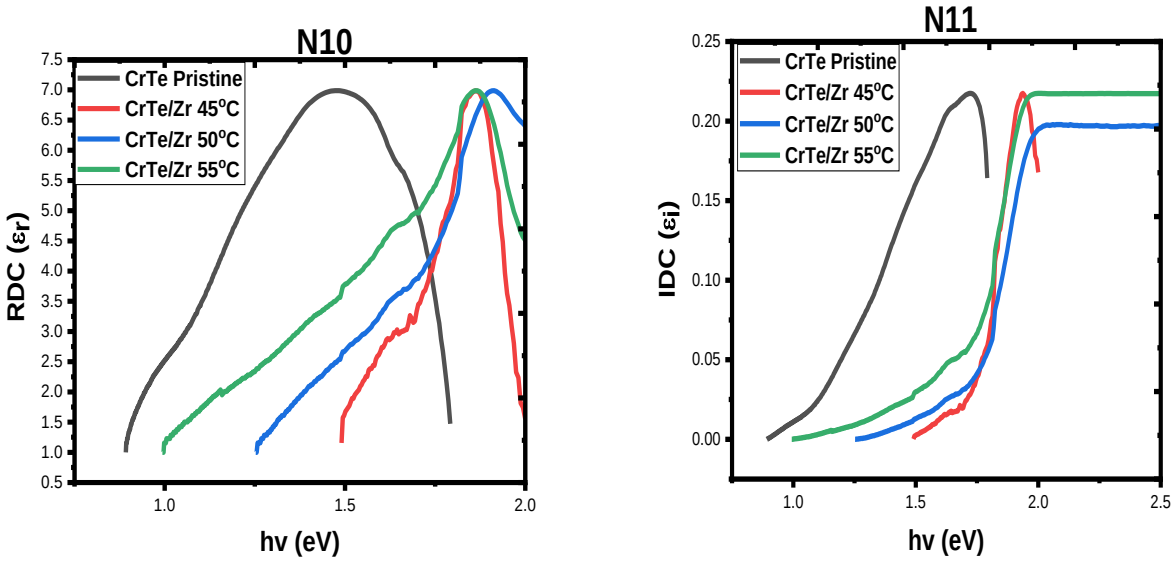

Figure 6: (N10-real dielectric constant) and (N11-imaginary dielectric constant)

3.4 Surface morphology of CrTe and Zr/CrTe

In the micrograph of CrTe and Zr/CrTe in Figure 7, the agglomeration on the films without pinholes and the densely packed grain size are visible. The CrTe image shows a well-packed shaving surface with condensed particles. Due to the tightly packed grain size, the substrate's surface exhibits photon absorption, but there are no apparent pinholes. The surface morphology of the films has revealed the smote surface with obvious stone dot micro grain that was detected as the precursor reaches a temperature of 50°C. The surface of the doped CrTe material displayed uniform nano-grain deposition. They will be a strong candidate for photovoltaic and other applications in the electronic industries since the surface microstructure of the zirconium doped films is perfectly ordered on the surface of the FTO substrate used for manufacturing and free from any fracture or lattice strain. The elemental spectra of the CrTe and Zr/CrTe films are shown in Figure 8. The spectrum demonstrates unequivocally that the dopant chromium, tellurium, and zirconium each exhibit distinctive peaks. The others element visible on the spectrum is the fundamental component of the FTO substrate.

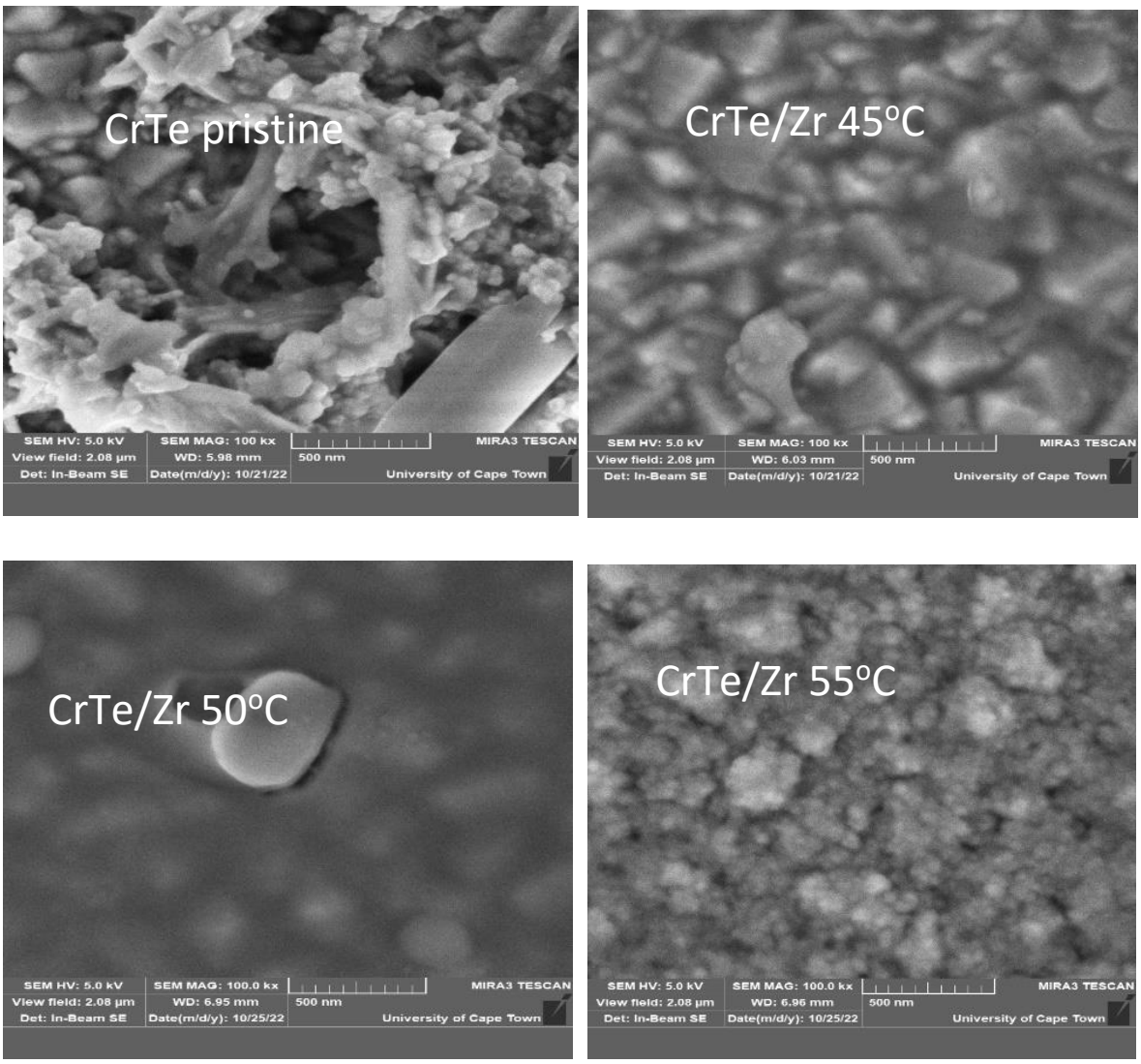

Figure 7: Surface image of CrTe and Zr/CrTe

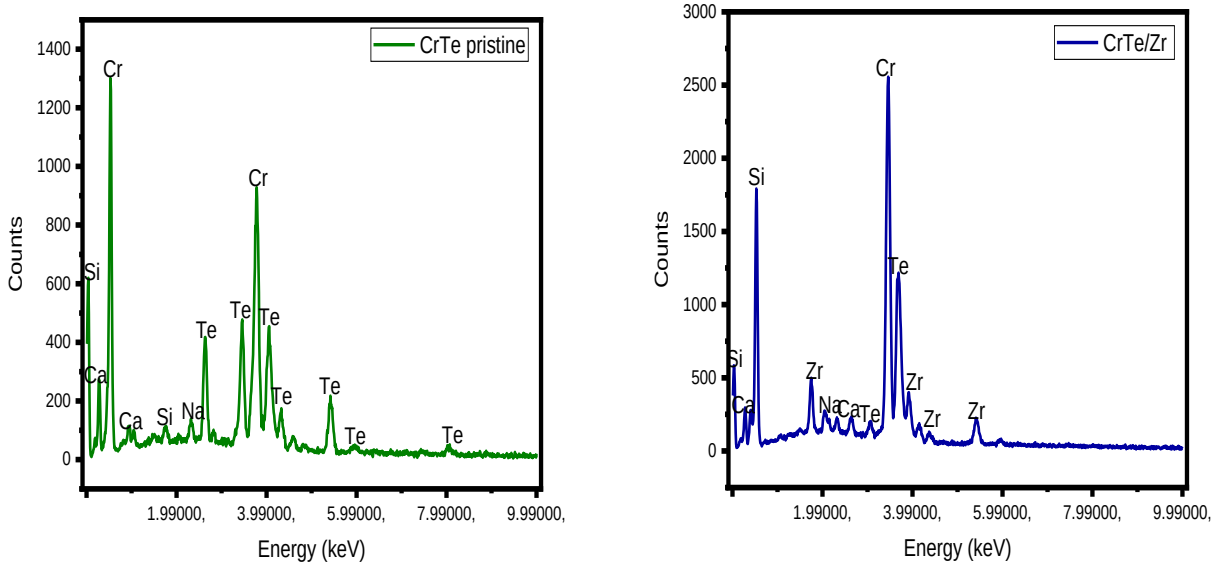

Figure 8: EDX spectrum of CrTe and Zr/CrTe

Conclusion

By adjusting the precursor temperature of the films, we were able to produce CrTe and Zr/CrTe using the electrochemical deposition method. The materials used to synthesize the films are polycrystalline. The material showed a prominent peak at orientation (121), which corresponds to a 2theta value of 46.92^{o}, together with a flawless hexagonal phase diffraction plane that is classified to orientations (111), (112), (121), and (200), which correspond to 2theta values of 21.57^{o}, 32.20^{o}, 46.92^{o}, and 60.02^{o}. An intensity peak indicates the crystal structure reduction that occurs at larger 2theta degree values; the substrate used for the deposition caused an unindexed peak. The films show a rise in thickness from 104.02 to 109.23 nm and a decrease in film resistivity from 7.68 x 10^{-3} to 7.34 x 10^{-3} ohm.m, which further led to an increase in conductivity from 1.30 x 10^{6} to 1.36 x 10^{-3} S/m. The undoped film's reflectance is highest in the visible region and gradually decreases until it approaches the near-infrared region. The reflectance of the films decreases in the UV region while the precursor temperatures rise along with the increase in reflectance in the visible area. The CrTe image shows a well-packed shaving surface with condensed particles. Due to the tightly packed grain size, the substrate's surface exhibits photon absorption, but there are no apparent pinholes. The surface morphology of the films has revealed the smote surface with obvious stone dot micro grain that was detected as the precursor reaches a temperature of 50°C. The surface of the doped CrTe material displayed uniform nano-grain deposition. The CrTe pristine has a bandgap energy of 1.62 eV, and Zr/CrTe synthesized at a different precursor temperature, has a bandgap energy of 1.73-1.68 eV, demonstrating that as the precursor temperature rises, the energy bandgap decreases.

Declarations

Funding: For this research, the authors were not given any funding.

Conflicts of Interest: No apparent conflicts of interest

Ethical Statement: The authors' research and analysis are fully and accurately reflected in the publication.

Data Availability Statement: The data supporting the study's conclusions are available upon request from the corresponding author.

Author Statement

Ernest O. Ojegu, Ogo B. Odia, and Imosobomeh L. Ikhioya: Conceptualization, methodology, experimentation, writing the original draft. **Imosobomeh L. Ikhioya:** re-writing original draft, Graphical work, and reference, **Mike O. Osiele, Akpojotor E. Godfrey** : investigation and supervisions

Reference

Al-Ghamdi A.A., Khan S. A., Nagat A., Abd El-Sadek M.S. (2010) Synthesis and optical characterization of nanocrystalline CdTe thin films, *Optics & Laser Technology*, 42(8), 1181-1186, ISSN 0030-3992, https://doi.org/10.1016/j.optlastec.2010.03.007

Arbouch I., Karzazi Y., Hammouti B. (2014) Organic photovoltaic cells: Operating principles, recent developments and current challenges–review *Phys. Chem. News* 72 (4), 73-84

Barhoum A., García-Betancourt M.L., Jeevanandam J., Hussien E.A., Mekkawy S.A., Mostafa M., Omran M.M., S. Abdalla M., Bechelany M. (2022) "Review on Natural, Incidental, Bioinspired, and Engineered Nanomaterials: History, Definitions, Classifications, Synthesis, Properties, Market, Toxicities, Risks, and Regulations," *Nanomaterials*, 12(2), Art. 2, doi:10.3390/nano12020177.

Chen C., X. Chen, C. Wu, Xiao Wang, Yue Ping, Xin Wei, Xing Zhou, Jiangbo Lu, Lujun Zhu, Jiadong Zhou, Tianyou Zhai, Junbo Han and Hua Xu. (2022) Air-Stable 2D Cr 5 Te 8 Nanosheets with Thickness-Tunable Ferromagnetism. *Advanced Materials*, 34, 2107512 DOI: 10.1002/adma.202107512

Hala. S. Hussein, (2023) "The state of the art of nanomaterials and its applications in energy saving," *Bulletin of the National Research Centre*, 47, 1, 7, doi: 10.1186/s42269-023-00984-4.

Hongxi Li, Linjing Wang, Junshu Chen, Tao Yu, Liang Zhou, Yang Qiu, Hongtao He, Fei Ye, Iam Keong Sou, and Gan Wang. (2019) Molecular Beam Epitaxy Grown Cr2Te3 Thin Films with Tunable Curie Temperatures for Spintronic Devices. *ACS Applied Nano Materials*, 2 (11), 6809-6817. DOI: 10.1021/acsanm.9b01179

Hui L. and T. K. Leong, (2013) "Investigation of rock-salt CrTe thin film grown by molecular beam epitaxy toward half-metal," 2013 IEEE 5th International Nanoelectronics Conference (INEC), Singapore, 56-58, doi: 10.1109/INEC.2013.6465952.

Ikhioya I. L., Okoli D. N., Ekpunobi A. J, (2020) "The Influence of Precursor Temperature on the Properties of Erbium-Doped Zirconium Telluride Thin Film Material via Electrochemical Deposition," *SSRG International Journal of Applied Physics*, 7, 1, 102-109. http://dx.doi.org/10.14445/23500301/IJAP-V7I1P115

Ikhioya I.L., and Azubike Josiah Ekpunobi, (2015) "Electrical and Structural properties of ZnSe Thin Films by Electrodeposition Technique," Journal of Nigeria Association of Mathematical Physics, 29, 325-330.

Ikhioya I. L., Ekpunobi A. J., Okoli D. N, (2020) "Effect of Precursor pH on Cadmium Doped Manganese Sulphide (CdMnS) Thin Films for Photovoltaic Application," SSRG International Journal of Applied Physics, 6, 2, 1-8. https://doi.org/10.14445/23948884/IJMSE-V6I2P101

Ikhioya I. L., Okoli D. N, and Ekpunobi A. J, (2019) "Effect of Temperature on SnZnSe Semiconductor Thin Films for Photovoltaic Application," SSRG International Journal of Applied Physics, 6, 2, 55-67 https://doi.org/10.14445/23500301/IJAP-V6I2P109

Ikhioya I.L, Goodfriend M. Whyte, and Agnes C.Nkele, "Temperature-Modulated Nanostructures of Ytterbium-Doped Cobalt Selenide (Yb-CoSe) for Photovoltaic Applications," Journal of the Indian Chemical Society, 100, 1, 100848. https://doi.org/10.1016/j.jics.2022.100848

Ikhioya I.L., and Azubike Josiah Ekpunobi, (2014) "Effect of Deposition Period and pH on Electrodeposition Technique of Zinc Selenide Thin Films," *Journal of Nigeria Association of Mathematical Physics*, 28, 2, 281-288.

Ikhioya I.L., Ugbo F. C, and Ijabor B. Okeghene, (2018) "Growth and Characterization of Manganese Sulphide (MnS) Thin Films," *International Journal for Research in Applied and Natural Science*, 4, 1, 1-9. https://doi.org/10.53555/ans.v4i1.77

Jafari M., Nowak D.B., Huang S., Abrego J.C., Yu T., Du Z., Ma D., Hammouti B., Jeffali F., Siaj M. (2023) Photo-induced force microscopy applied to electronic devices and biosensors, *Mater. Today Proc.*, 72 (Part7), 3904-3910, doi.org/10.1016/j.matpr.2022.10.216

Jiang X., F. Chen, S. Zhao and W. Su. (2021) Recent progress in the CVD growth of 2D vertical heterostructures based on transition-metal dichalcogenides. *Cryst. Eng. Comm.*, 23,8239 DOI: 10.1039/D1CE01289D

Luo F., J. Ying, Y. Zhang, S. Li, Fang Tang, Ting-Wei Chen, Zhao-Cai Wang, Shu-Juan Zhang, Yong Fang and Ren-Kui Zheng. (2022) The effects of substrate temperature on the magnetic and magnetotransport properties of Cr1-Te epitaxial films. *Journal of Magnetism and Magnetic Materials*, 550,169084. DOI: 10.1016/j.jmmm.2022.169084

Mobeen, H. M. Safdar, A. Fatima, S. Afzal, H. Zaman, and Z. Mehdi, (2022) "Emerging applications of nanotechnology in context to immunology: A comprehensive review," *Frontiers in Bioengineering and Biotechnology*, 10, 1024871, doi:10.3389/fbioe.2022.1024871.

Mote V. D., J. S. Dargad, Y. Purushotham, and B. N. Dole, (2015) "Effect of doping on structural, physical, morphological and optical properties of Zn1−xMnxO nano-particles," *Ceramics International*, 41, 10, Part B, 15153–15161, doi:10.1016/j.ceramint.2015.08.088.

Polat O. *et al.*, (2019) "Tailoring the band gap of ferroelectric YMnO3 through tuning the Os doping level," *J. Mater. Sci: Mater. Electron.*, 30, 4, 3443–3451, doi:10.1007/s10854-018-00619-9.

Sreenivasan M.G., X.J. Hou, K.L. Teo, M.B.A. Jalil, T. Liew, T.C. Chong, (2006) Growth of CrTe thin films by molecular-beam epitaxy, *Thin Solid Films*, 505, 1–2, 133-136. https://doi.org/10.1016/j.tsf.2005.10.027

Su R., Xu Z., Wu J. et al. (2021). Dielectric screening in perovskite photovoltaics, *Nat. Commun.* 12, 2479 https://doi.org/10.1038/s41467-021-22783-z

Sun S, J. Liang, R. Liu, W. Shen, H. Wu, M. Tian, Lulu Cao, Yutian Yang, Zhaocong Huang, Weiwei Lin, Jun Du, Zhenhua Ni, Yongbing Xu, Qian Chen and Ya Zhai. (2022) Anisotropic magnetoresistance in room temperature ferromagnetic single crystal CrTe flake. *Journal of Alloys and Compounds*, 890, 161818; DOI: 10.1016/j.jallcom.2021.161818

Sven K., H. Sabine, B. Wolfgang. (2002) Low-temperature synthesis of chromium tellurides using superlattice reactants: crystallization of layered CrTe3 at 100◦C and the decomposition into Cr2Te3, *Solid State Sciences* 4,1237–1243

Udofia K. I. *et al.*, (2022) "Effects of Zirconium on Electrochemically Synthesized Tin Selenide Materials on Fluorine Doped Tin Oxide Substrate for Photovoltaic Application," *Journal of the Indian Chemical Society*, 99, 10, 10077. https://doi.org/10.1016/j.jics.2022.100737

Wang J., B. Zhang, M. Shen et al., (2011) "Effects of Fe-doping of ceria-based materials on their microstructural and dynamic oxygen storage and release properties," *Journal of Sol-Gel Science and Technology*, 58, 1, 259–268.

Wang Y., S. Kajihara, H. Matsuoka, B. Kenichi Saika, Kohei Yamagami, Yukiharu Takeda, Hiroki Wadati, Kyoko Ishizaka, Yoshihiro Iwasa and Masaki Nakano. (2022) Layer-Number-Independent Two-Dimensional Ferromagnetism in Cr3Te4. *Nano Lett.*, 22, 9964 DOI: 10.1021/acs.nanolett.2c03532

Yang H., A.Wu, H. Yi, W. Cao, J. Yao, G.Yang and Y. Zou. (2023) Atomic scale insights into the epitaxial growth mechanism of 2D Cr3Te4 on mica, *Nanoscale Adv.*, 5, 693. DOI: 10.1039/D2NA00835A

Yang Y., L. Jia, D. Wang and J. Zhou. (2023) Advanced Strategies in Synthesis of Two-Dimensional Materials with Different Compositions and Phases. *Small Methods*, 7 DOI: 10.1002/smtd.202201585

Yuxi Guo, Lixing Kang, Shaojia Yu, Jiefu Yang, Xiaofei Qi, Zhiyong Zhang and Zheng Liu. (2021) CVD Growth of Large-scale and Highly Crystalline 2D Chromium Telluride Nanoflakes. *Chem. Nano. Mat.*, 7,323. DOI: 10.1002/cnma.202000650

Zhang S., H. Wu, L. Yang, G. Zhang, Y. Xie, L. Zhang, W. Zhang and H. Chang. (2022) Two-dimensional magnetic atomic crystals. *Mater. Horiz.*, 9, 559 DOI: 10.1039/D1MH01155C